Moving force identification based on modified preconditioned conjugate gradient method

Zhen Chen[a,b,*], Tommy H.T. Chan[b] , Andy Nguyen[b,c]

[a] *School of Civil Engineering and Communication, North China University of Water Resources and Electric Power, Zhengzhou 450045, China*
[b] *School of Civil Engineering and Built Environment, Queensland University of Technology (QUT), Brisbane 4000, Australia*
[c] *School of Civil Engineering and Surveying, University of Southern Queensland (USQ), Springfield Central 4300, Australia*

Abstract: This paper develops a modified preconditioned conjugate gradient (M-PCG) method for moving force identification (MFI) by improving the conjugate gradient (CG) and preconditioned conjugate gradient (PCG) methods with a modified Gram-Schmidt algorithm. The method aims to obtain more accurate and more efficient identification results from the responses of bridge deck caused by vehicles passing by, which are known to be sensitive to ill-posed problems that exist in the inverse problem. A simply supported beam model with biaxial time-varying forces is used to generate numerical simulations with various analysis scenarios to assess the effectiveness of the method. Evaluation results show that regularization matrix **L** and number of iterations *j* are very important influence factors to identification accuracy and noise immunity of M-PCG. Compared with the conventional counterpart SVD embedded in the time domain method (TDM) and the standard form of CG, the M-PCG with proper regularization matrix has many advantages such as better adaptability and more robust to ill-posed problems. More importantly, it is shown that the average optimal numbers of iterations of M-PCG can be reduced by more than 70% compared with PCG and this apparently makes M-PCG a preferred choice for field MFI applications.

Keywords: moving force identification; modified preconditioned conjugate gradient; time domain method; regularization matrix; number of iterations; modified Gram-Schmidt algorithm

1. Introduction

Advances in structural health monitoring of bridges have driven research into inverse problems involving system parameter identification, damage detection, and dynamic state estimation in vehicle-bridge system [1,2]. Amongst these, moving force identification (MFI) is a representative inverse problem of vehicle-bridge system that has drawn much the attention from many researchers in the past two decades. The rationale for MFI applications is that it is often very difficult or even impossible to measure dynamic loads directly, which leads to the booming development of the theory of load identification [3].

*Corresponding author.
E-mail address: yuchenfish@163.com; z45.chen@qut.edu.au (Z. Chen).

Chan et al developed interpretive method I (IMI) [4], interpretive method II (IMII) [5], time domain method (TDM) [6] and frequency-time domain method (FTDM) [7] in the past two decades and conducted series in-depth studies with these four methods [8-11]. Computation simulations and laboratory tests show that the TDM and FTDM are clearly better than those from both IMI and IMII [12]. Law et al [13] indicated that the TDM was better than FTDM in solving for the ill-posed problem. Liu et al [3] also indicated that compared with frequency-domain methods, methods in time domain have clearer physical meaning and relatively higher accuracy, which can be used to identify various types of loads and have a good prospect in engineering. Therefore, the TDM is a widely used method which has been improved by some researchers [14-15]. The singular value decomposition (SVD) of the coefficient matrix of the overdetermined equation has been introduced in FTDM [16] and TDM [17] to improve the identification accuracy. However, it was still found that the identified accuracy of many methods is sensitive to noise and exhibit large fluctuations, since the nature of the complex inverse problem is inherent ill-posed [18], which rationalizes the ongoing effort of many researchers in deriving new methods to overcome the ill-posedness of MFI.

Sanchez et al [19] indicated that the ill-posedness of MFI is problematic since noise becomes very influential and results in inaccurate or non-unique solutions. To combat this ill-posedness, additional constraints are typically applied to redefine the problem, leading to a well-defined problem with a unique solution. Pinkaew [20] presented an updated static component (USC) technique to solve the accuracy of the identified results is very sensitive to the vehicle-bridge properties. González et al. [21] introduced an algorithm based on first order Tikhonov regularization to overcome the impact of noise in strain responses. Yu et al. [22,23] proposed an algorithm of moments (MOM) and a weighted l_1-norm regularization method to acquire an acceptable solution to the ill-posed problem that often exists in the inverse problem of MFI. Wu et al. [24] developed a MFI technique based on a statistical system model. Dowling et al. [25] adopted cross entropy optimization method to calibrate the vehicle-bridge system matrices required of the MFI algorithms. Feng et al. [26] used a Bayesian inference regularization approach to solve the ill-posed least squares problem for input axle loads. Chen et al. [27] presented a truncated generalized singular value decomposition method (TGSVD) aims at obtaining an acceptable solution of MFI and making the noise to be less sensitive to perturbations with the ill-posed problems.

As mentioned earlier, methods in time domain have clear physical meaning, relatively higher accuracy and stronger immunity of ill-posed problem compared with frequency-domain methods. In the time domain, the MFI problem eventually becomes solving the linear algebraic equation which can be dealt with by least square approximation methods. In linear algebra, the conjugate gradient (CG) algorithm is a well-known iterative method proposed by Hestenes and Stiefel in 1952 [28]. The CG process has some inherent regularization effect

which can be used to combat the ill-posedness for solving sparse systems equation [29]. Concus et al. [30] proposed the block preconditioning for the CG method and indicated that a particularly attractive preconditioning, which uses special properties of tridiagonal matrix inverses, can be computationally more efficient for the same computer storage than other preconditionings. Meurant et al. [31] introduced the Lanczos algorithm constructs a basis of Krylov subspaces to CG algorithm with deep links for solving linear algebraic equations. The CG algorithm and the preconditioned conjugate gradient (PCG) algorithm have been widely used since their numerical behaviour can be explained by an elegant mathematical theory. Chen and Yu [32-34] presented a PCG algorithm for MFI and verified this method by experiment but the accuracy of the PCG under different iteration settings has not been investigated. In addition, there has been a lack of literature on the evaluation of different CG methods against each other as well as against other similar methods especially in regard to solving the MFI problem.

In this paper, based on the existing CG and PCG techniques, a modified preconditioned conjugate gradient (M-PCG) method is proposed for MFI aiming to overcome the ill-posed problems. In order to improve the computational accuracy and ill-posed immunity of PCG, the regularization matrix **L** and the number of iterations *j* are introduced and simulations are conducted to evaluate this modification. Furthermore, the iterative optimization of M-PCG also has been conducted under tight scrutiny to improve the computation efficiency by introducing the modified Gram-Schmidt (MGS) algorithm [35]. The simulation results show that the M-PCG has many advantages such as higher precision, better adaptability, more noise immunity and ill-posed immunity as compared to TDM when the regularization matrix **L** and the number of iterations *j* are selected properly. Moreover, the M-PCG can identify the moving load faster and more effectively compared with the PCG, resulting in the average optimal numbers of iterations reduced by more than 70%. These advantages of M-PCG will be very useful towards field applications to solve MFI problems.

2. Moving force identification theory

2.1. Theory of time domain method (TDM)

The bridge-vehicle system is modeled as a simply supported beam and subject to a time varying force as shown in Fig.1. The load $f(t)$ is assumed moving at a prescribed velocity c at time t, along the axial direction of the beam from left to right. The equation of motion in terms of the modal coordinate $q_n(t)$ can be written as

$$\ddot{q}_n(t) + 2\xi_n\omega_n\dot{q}_n(t) + \omega_n^2 q_n(t) = \frac{2}{\rho L}p_n(t), \quad (\mathrm{n} = 1,2,\dots,\infty) \tag{1}$$

where L is the span length of the beam; ρ is the constant mass per unit length; $p_n(t) = f(t)\sin\frac{n\pi ct}{L}$ is the modal force; $\omega_n = \frac{n^2\pi^2}{L^2}\sqrt{\frac{EI}{\rho}}$ is the nth modal frequency; E is the Young's

modulus; I is the second moment of inertia of the beam cross-section; $\xi_n = \frac{C}{2\rho\omega_n}$ is the modal damping ratio and C is the viscous damping.

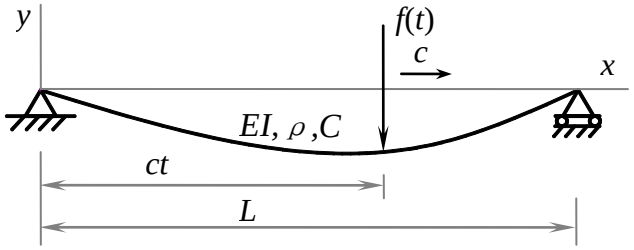

Fig.1. Moving force identification model with a simply supported beam

Based on modal superposition, the deflection $v(x,t)$ of the beam at point x and time t can be described as Law et al. [6]

$$v(x,t) = \sum_{n=1}^{\infty} \frac{2}{\rho L \omega_n'} \sin\frac{n\pi x}{L} \int_0^t e^{-\xi_n\omega_n(t-\tau)} \sin\omega_n'(t-\tau) \sin\frac{n\pi c\tau}{L} f(\tau)\mathrm{d}\tau \tag{2}$$

where $\omega_n' = \omega_n\sqrt{1-\xi_n^2}$ and the bending moment $M(x,t)$of the beam at point x and time t is

$$M(x,t) = -EI\frac{\partial^2 v(x,t)}{\partial x^2} = \sum_{n=1}^{\infty} \frac{2EI\pi^2}{\rho L^3}\frac{n^2}{\omega_n'} \sin\frac{n\pi x}{L} \int_0^t e^{-\xi_n\omega_n(t-\tau)} \sin\omega_n'(t-\tau) \sin\frac{n\pi c\tau}{L} f(\tau)\mathrm{d}\tau \tag{3}$$

The acceleration $\ddot{v}(x,t)$ of the beam at point x and time t also can be described as

$$\ddot{v}(x,t) = \sum_{n=1}^{\infty} \frac{2}{\rho L} \sin\frac{n\pi x}{L} \left[f(t)\sin\frac{n\pi x}{L} + \int_0^t \ddot{h}_t(t-\tau) f(\tau) \sin\frac{n\pi c\tau}{L}\mathrm{d}\tau\right] \tag{4}$$

where $\ddot{h}_n(t) = \frac{1}{\omega_n'} e^{-\xi_n\omega_n t} \times \{[(\xi_n\omega_n)^2 - \omega_n'^2]\sin\omega_n' t + (-2\xi_n\omega_n\omega_n')\cos\omega_n' t\}$.

If the bending moment responses are measured, the moving force **f** can be identified by equation $\mathbf{B}\cdot\mathbf{f} = \mathbf{M}$. Similarly, if the acceleration responses are measured, the moving force **f** can be identified by equation $\mathbf{A}\cdot\mathbf{f} = \ddot{\mathbf{V}}$. If the bending moment and acceleration responses are measured at the same time, both of them can be used together to identify the moving force. The vector **M** and $\ddot{\mathbf{V}}$ should be scaled to make them dimensionless, and the two equations are then combined to give

$$\begin{bmatrix} \mathbf{B}/\|\mathbf{M}\| \\ \mathbf{A}/\|\ddot{\mathbf{V}}\| \end{bmatrix} \times \mathbf{f} = \begin{Bmatrix} \mathbf{M}/\|\mathbf{M}\| \\ \ddot{\mathbf{V}}/\|\ddot{\mathbf{V}}\| \end{Bmatrix} \tag{5}$$

where $\|\cdot\|$ is the norm of the vector; **B** and **A** are the vehicle-bridge system matrix; **M** and $\ddot{\mathbf{V}}$ are the bending moment and acceleration responses matrix, respectively.

2.2. Theory of conjugate gradient (CG)

In the time domain, the MFI problem eventually converts to a linear algebraic equation in the form $\mathbf{Ax} = \mathbf{b}$, where $\mathbf{A} \in \mathbf{R}^{m\times n}$, $\mathbf{x} \in \mathbf{R}^n$, $\mathbf{b} \in \mathbf{R}^m$, $m \geq n$. The **A** is vehicle-bridge system matrix, the vector **b** is measured responses of bridge structures contaminated by an unknown

error stemming from measurement error. The CG algorithm is an iterative method which terminates in at most j steps if no rounding-off error is encountered. With number of iterations j, the approximations moving force $\mathbf{x}_j$ can be obtained and the residual $\mathbf{r}_j = \mathbf{b} - \mathbf{A}\mathbf{x}_j$. In case the matrix $\mathbf{A}$ is symmetric and positive definite, by defining $\mathbf{p}_0 = \mathbf{r}_0 = \mathbf{b} - \mathbf{A}\mathbf{x}_0$, where $\mathbf{x}_0$ is arbitrary initial moving force, the jth step of the CG process can be expressed as giving coefficients α_j and β_j used to update the iteration vectors [28]

$$\alpha_j = \frac{(\mathbf{p}_j, \mathbf{r}_j)}{(\mathbf{p}_j, \mathbf{A}\mathbf{p}_j)}$$
$$\beta_j = -\frac{(\mathbf{r}_{j+1}, \mathbf{A}\mathbf{p}_j)}{(\mathbf{p}_j, \mathbf{A}\mathbf{p}_j)} \tag{6}$$

where

$$\begin{aligned} \mathbf{r}_j &= \mathbf{r}_{j-1} - \alpha_{j-1}\mathbf{A}\mathbf{p}_{j-1} \\ \mathbf{p}_j &= \mathbf{r}_j + \beta_{j-1}\mathbf{p}_{j-1} \\ \mathbf{x}_j &= \mathbf{x}_{j-1} + \alpha_{j-1}\mathbf{p}_{j-1} \end{aligned} \tag{7}$$

in which $\mathbf{x}_j$ is the approximation to $\mathbf{x}$ after j-th iterations, while $\mathbf{p}_j$ is an auxiliary iteration vector of length n.

2.3. Theory of preconditioned conjugate gradient (PCG)

As mentioned above, the CG process is based on the matrix $\mathbf{A}$ is symmetric positive definite coefficient matrix. When the matrix $\mathbf{A}$ is nonsymmetric and nonsingular matrix, the CG process can be extended by using $\mathbf{A^T A}$ replace the matrix $\mathbf{A}$ and using equation $\mathbf{A^T A x} = \mathbf{A^T b}$ replace the equation $\mathbf{A x} = \mathbf{b}$. To explain this regularizing effect of the CG method, Concus et al. [30] introduced the Krylov subspace to CG method

$$\mathcal{K}_k\left(\mathbf{A^T A}, \mathbf{A^T b}\right) = \text{span}\left\{\mathbf{A^T b}, \mathbf{A^T A A^T b}, \cdots, \left(\mathbf{A^T A}\right)^{k-1}\mathbf{A^T b}\right\} \tag{8}$$

Then the CG method can be rewritten to solve the following problem

$$\mathbf{x}_j = \text{argmin}\|\mathbf{A}\mathbf{x} - \mathbf{b}\|_2 \quad \text{subject to} \quad \mathbf{x} \in \mathcal{K}_k\left(\mathbf{A^T A}, \mathbf{A^T b}\right) \tag{9}$$

The primary difficulty with the MFI ill-posed problem is that it is essentially underdetermined due to the cluster of small singular values of vehicle-bridge system matrix $\mathbf{A}$. Hence, it is necessary to incorporate further information about the CG process in order to stabilize the problem and to single out a useful and stable solution. For ill-posed inverse problems, the preconditioning represents an unavoidable and fundamental part of practical computations. A sparse approximate inverse preconditioner for an unsymmetric matrix $\mathbf{A}$ may be obtained by constructing a set of approximate biconjugate directions for $\mathbf{A}$ [36]. Then the preconditioned conjugate gradient method (PCG) is introduced by adopting the regularization matrix $\mathbf{L}$.

Assuming that the initial estimate moving force is the $\mathbf{x}^*$, the dominating approach to regularization of MFI ill-posed problems is to require that the 2-norm of the solution be small. Hence, the side constraint $\Omega(\mathbf{x})$ involves minimization of the quantity

$$\Omega(\mathbf{x}) = \|\mathbf{L}(\mathbf{x} - \mathbf{x}^*)\|_2 \tag{10}$$

Here, the matrix $\mathbf{L}$ is typically either the unit matrix $\mathbf{I}_n$ or a $p \times n$ discrete approximation of the $(n-p)$-th derivative operator, in which case $\mathbf{L}$ is a banded matrix with full row rank. As $\mathbf{L}_1 = \mathbf{I}_n$, based on the finite difference methods for the derivatives, $\mathbf{L}_2$, $\mathbf{L}_3$, $\mathbf{L}_4$ and $\mathbf{L}_5$ are approximations to the first, second, third and fourth derivative operators with null space as shown in equation (11). The proper choice of matrix $\mathbf{L}$ depends on the particular application, but often an approximation to the first or second derivative operator gives good results [37].

$$\mathbf{L_1} = \begin{pmatrix} 1 & & & \\ & 1 & & \\ & & \ddots & \\ & & & 1 \end{pmatrix}_{n\times n}$$

$$\mathbf{L_2} = \begin{pmatrix} -1 & 1 & & & \\ & -1 & 1 & & \\ & & \ddots & \ddots & \\ & & & -1 & 1 \end{pmatrix}_{(n-1)\times n} \tag{11}$$

$$\mathbf{L_3} = \begin{pmatrix} 1 & -2 & 1 & & \\ & 1 & -2 & 1 & \\ & & \ddots & \ddots & \ddots \\ & & & 1 & -2 & 1 \end{pmatrix}_{(n-2)\times n}$$

$$\mathbf{L}_4 = \begin{pmatrix} -1 & 3 & -3 & 1 & & \\ & -1 & 3 & -3 & 1 & \\ & & \ddots & \ddots & \ddots & \ddots \\ & & & -1 & 3 & -3 & 1 \end{pmatrix}_{(n-3)\times n}$$

If the matrix $\mathbf{L}$ is the unit matrix $\mathbf{I_n}$, i.e., there is no regularization process, then the PCG is essentially the form of CG and the regularization problem with side constraint in equation (10) is standard form. However, in MFI applications, regularization in standard form is not the best choice, i.e., one should use some $\mathbf{L} \neq \mathbf{I}_n$ in equation (10). If the matrix $\mathbf{L}$ is the first or second derivative operator, then the PCG is general form. From numerical point of view, the standard form is much simpler to treat problems compared with general form as only one matrix $\mathbf{A}$ is involved instead of the two matrices $\mathbf{A}$ and $\mathbf{L}$. Hence, it is convenient to transform the general form into standard form.

The singular value decomposition (SVD) of bridge-vehicle system matrix $\mathbf{A}$ can be expressed with two orthonormal columns matrices $\mathbf{U} = (\mathbf{u}_1, \mathbf{u}_2, \cdots \mathbf{u}_n)$ and $\mathbf{V} = (\mathbf{v}_1, \mathbf{v}_2, \cdots \mathbf{v}_n)$ as $\mathbf{A} = \mathbf{U\Sigma V}^T = \sum_{i=1}^{n} \mathbf{u}_i \, \boldsymbol{\sigma}_i \mathbf{v}_i^T$ .The $\sum = \mathrm{diag}(\sigma_1, \sigma_2, \cdots, \sigma_n)$ has non-negative diagonal elements, which is constituted with the singular values σ_i as $\sigma_1 \geq \sigma_2 \geq \cdots \geq \sigma_n \geq 0$.

By introducing $\bar{\mathbf{A}} = \mathbf{A}\mathbf{L}_{\mathbf{A}}^{+}$, $\bar{\mathbf{b}} = \mathbf{b} - \mathbf{A}\mathbf{x}_0$ and $\bar{\mathbf{x}} = \mathbf{L}\mathbf{x}$, the general form of equation can be transformed into standard form. The $\mathbf{L}_{\mathbf{A}}^{+}$ is $\mathbf{A}$-weighted generalized inverse of $\mathbf{L}$ as, which can be expressed as

$$\mathbf{L}_{\mathbf{A}}^{+} = \mathbf{X}\begin{pmatrix}\mathbf{M}^{-1} \\ 0\end{pmatrix}\mathbf{V}^{T} \tag{12}$$

where the vector $\mathbf{x}_0 = \sum_{i=p+1}^{n}\left(\mathbf{u}_i^T\mathbf{b}\right)\mathbf{x}_i$, p is the rows of matix $\mathbf{L}$. Then the Krylov subspace of PCG algorithm can be written to solve the following problem

$$\bar{\mathbf{x}}_j = \operatorname{argmin}\left\|\bar{\mathbf{A}}\bar{\mathbf{x}} - \bar{\mathbf{b}}\right\|_2 \quad \text{subject to} \quad \bar{\mathbf{x}} \in \mathcal{K}_k\left(\bar{\mathbf{A}}^{\mathbf{T}}\bar{\mathbf{A}}, \bar{\mathbf{A}}^{\mathbf{T}}\bar{\mathbf{b}}\right) \tag{13}$$

The j-th iterate of PCG algorithm can be written as

$$\bar{\mathbf{x}}_j = \mathcal{R}_j\left(\bar{\mathbf{A}}^{\mathbf{T}}\bar{\mathbf{A}}\right)\bar{\mathbf{A}}^{\mathbf{T}}\bar{\mathbf{b}} \tag{14}$$

where $\mathcal{R}_j$ is a polynomial of degree $j-1$ satisfying the following recurrence relation and with initial conditions $\mathcal{R}_0 = \mathcal{R}_{-1} = 0$

$$\mathcal{R}_j = \left(1 - \theta\alpha_j + \frac{\alpha_j\beta_{j-1}}{\alpha_{j-1}}\right)\mathcal{R}_{j-1} - \frac{\alpha_j\beta_{j-1}}{\alpha_{j-1}}\mathcal{R}_{j-2} + \alpha_j \tag{15}$$

where θ is Ritz value related to eigenvalues of matrix $\mathbf{A}$, with $\bar{\mathbf{A}} = \mathbf{A}\mathbf{L}_{\mathbf{A}}^{+}$ and $\bar{\mathbf{b}} = \mathbf{b} - \mathbf{A}\mathbf{x}_0$ insert into the equation (14), it can be rewritten as

$$\bar{\mathbf{x}}_j = \mathcal{R}_j\left((\mathbf{L}_{\mathbf{A}}^{+})^T\mathbf{A}^{\mathbf{T}}\mathbf{A}\mathbf{L}_{\mathbf{A}}^{+}\right)(\mathbf{L}_{\mathbf{A}}^{+})^T\mathbf{A}^{\mathbf{T}}(\mathbf{b} - \mathbf{A}\mathbf{x}_0) \tag{16}$$

With $\mathbf{x}_j = \mathbf{L}_{\mathbf{A}}^{+}\bar{\mathbf{x}}_j + \mathbf{x}_0$ and $(\mathbf{L}_{\mathbf{A}}^{+})^T\mathbf{A}^{\mathbf{T}}\mathbf{A}\mathbf{x}_0 = \mathbf{0}$, the j iterative steps of PCG method $\mathbf{x}_j$ can be obtained as

$$\mathbf{x}_j = \mathcal{R}_j\left(\mathbf{L}_{\mathbf{A}}^{+}(\mathbf{L}_{\mathbf{A}}^{+})^T\mathbf{A}^{\mathbf{T}}\mathbf{A}\right)\mathbf{L}_{\mathbf{A}}^{+}(\mathbf{L}_{\mathbf{A}}^{+})^T\mathbf{A}^{\mathbf{T}}\mathbf{b} + \mathbf{x}_0 \tag{17}$$

From this relation, the purpose of the "preconditioner" is not to improve the condition of the iteration matrix but rather to ensure that the "preconditioned" iteration vector $\mathbf{x}_j$ lies in the correct subspace and thus minimizes the residual norm of $\|\mathbf{A}\mathbf{x} - \mathbf{b}\|_2$. The regularization matrix $\mathbf{L}$ and the number of iterations j in equation (17) are introduced to improve the computational accuracy and ill-posed immunity of PCG.

2.4. Theory of modified preconditioned conjugate gradient (M-PCG)

Gram-Schmidt algorithm is named after Jorgen Pedersen Gram and Erhard Schmidt but it appeared earlier in the work of Laplace and Cauchy [38]. In mathematics, the Gram-Schmidt algorithm is a method for orthonormalising a set of vectors in an inner product space, most commonly the Euclidean space equipped with the standard inner product.

Let $\mathbf{A}$ be an $m \times n$ real matrix, $m \geq n$ of full rank n. In exact arithmetic, the modified Gram-Schmidt algorithm (MGS) computes an $m \times n$ matrix $\mathbf{Q}$ with orthonormal columns $\mathbf{Q}^T\mathbf{Q} = \mathbf{I}$ and an $n \times n$ upper triangular matrix $\mathbf{R}$ such that $\mathbf{A} = \mathbf{Q}\mathbf{R}$. Dax [39] presented the row-oriented iterative MGS by improving the classical Gram-Schmidt (CGS) and column-oriented MGS with iterative orthogonalization. The application of the CGS to the column vectors of a full column rank matrix yields the QR decomposition. This CGS loses accuracy when $\|\mathbf{r}_j\|_2$ is small with respect to $\|\mathbf{b}\|_2$, so iterative orthogonalization is essential to ensure accurate computation of small residuals. The difference between the algorithms lies in their

ability to orthogonalize the columns of vehicle-bridge system matrix **A**. The loss of orthogonality in the columns of **Q** can be avoided by repeated use of the orthogonalization process, which can be named as "reorthogonalization" and "iterative orthogonalization".

Many optimization problems are formulated with bounds on the variables, which cannot be treated directly by CG method. Comparing with several proposed modifications to CG method, it appears that the way the bounds are treated by optimization techniques has a significant impact on their efficiency [40]. The CGS and the MGS share the property that the matrices **Q** and **R** satisfy a bound of the form

$$\|\mathbf{A}-\mathbf{QR}\|_2 \leq \gamma\varepsilon\|\mathbf{A}\|_2 \tag{18}$$

where γ is a constant that depends on m and n, ε denotes the unit round-off.

The non-negative singular values of matrix **A** can be expressed as $\sigma_1 \geq \sigma_2 \geq \cdots \geq \sigma_n \geq 0$. The condition number of **A** is equal to the ratio $\frac{\sigma_1}{\sigma_n}$. If $\frac{\sigma_1}{\sigma_n} \ll \frac{1}{\varepsilon}$, then the MGS algorithm yields a matrix **Q** that satisfies [39]

$$\|\mathbf{I}-\mathbf{Q}^T\mathbf{Q}\|_2 \leq \gamma\varepsilon\frac{\sigma_1}{\sigma_n} \tag{19}$$

In other words, **Q** is guaranteed to be nearly orthogonal only when **A** is a well-conditioned matrix. The CGS fails to satisfy the bound of equation (19) and the columns of **Q** may depart from orthogonality to an almost arbitrary extent, which was observed by Rice [41]. The use of the MGS algorithm for solving linear least-squares problems ensures accurate computation of small residuals. A further advantage of the MGS is its ability to provide accurate results when **Q** has some deviation from orthogonality, which is beneficial to boost the iteration efficiency of iterative methods. For boosting the iteration efficiency of PCG, the bound equation (19) is appended to PCG to expedite the identification process and the new method is defined as modified preconditioned conjugate gradient (M-PCG).

3. Numerical simulation and rusults

3.1. Problem description

As shown in Fig.1, a simply supported beam subjected to a moving force is taken as an example for numerical simulations. The beam has a span of 40 m and the parameters of the beam are as follows: flexural rigidity EI $= 1.274916 \times 10^{11}$ N $\cdot$ m^2, density of unit length ρA $= 12\,000$kg $\cdot$ m^{-1}. The first three natural frequencies of the beam are 3.2 Hz, 12.8 Hz and 28.8 Hz. The analysis frequency is from 0Hz to 40Hz and the sampling frequency is 200Hz. The speed of moving vehicle is 40 m $\cdot$ s^{-1} and the distance between two axles is 4 m. The data are extracted from Law et al. [6] to enable comparison with the TDM derived in the paper. Biaxial time-varying forces identification with 12 different sensor arrangement and locations cases (1st column in Table 1) are simulated and illustrated with new method. The time history of the moving force is simulated as follow

$$f_1(t) = 20\,000[1 + 0.1\sin(10\pi t) + 0.05\sin(40\pi t)]\ \text{N}$$
$$f_2(t) = 20\,000[1 - 0.1\sin(10\pi t) + 0.05\sin(50\pi t)]\ \text{N}$$

Random noise is added into the calculated responses to simulate the polluted measurement responses in the following form

$$\mathbf{R}_{\text{measured}} = \mathbf{R}_{\text{calculated}} \cdot (1 + E_p \cdot \mathbf{N}_{\text{noise}}) \tag{20}$$

where E_p represents noise level choosing as 0.01, 0.05 and 0.10, respectively; $\mathrm{N}_{\text{noise}}$ is a standard normal distribution vector.

The relatively percentage error (RPE) values between the true moving force and the identified force are defined as follow

$$\mathrm{RPE} = \frac{\|\mathbf{f}_{\text{identified}} - \mathbf{f}_{\text{true}}\|}{\|\mathbf{f}_{\text{true}}\|} \times 100\% \tag{21}$$

where $\mathbf{f}_{\text{identified}}$, $\mathbf{f}_{\text{true}}$ are the identified force vector and true force vector, respectively.

3.2. Comparison with different regularization matrix **L** *of M-PCG*

The final stage in the regularization of ill-posed problems is the choice of regularization parameters. The identification accuracy and ill-posed immunity of M-PCG is profoundly affected if the regularization parameter is not correctly selected. The preconditioner $\mathbf{L}_\mathbf{A}^+(\mathbf{L}_\mathbf{A}^+)^T$ and the number of iterations *j* play an important role of regularization parameter, which should be chosen by numerical simulation prudently. In this part, the regularization matrix **L** of preconditioner $\mathbf{L}_\mathbf{A}^+(\mathbf{L}_\mathbf{A}^+)^T$ will be chosen. The RPE values of biaxial time-varying forces identified from combined responses (1/2m&1/4a&1/2a) by M-PCG with 8 different regularization matrices are shown in Fig.2. The abscissa values 1 to 8 are corresponding to regularization matrix $\mathbf{L}_1$ to $\mathbf{L}_8$, respectively. Illustration results demonstrate that the regularization matrices $\mathbf{L}_2$, $\mathbf{L}_3$ and $\mathbf{L}_4$ are much suitable matrices of M-PCG compared with others. In addition, the RPE values of $\mathbf{L}_2$ and $\mathbf{L}_3$ are slightly lower than $\mathbf{L}_4$, and then the $\mathbf{L}_2$ and $\mathbf{L}_3$ are chosen as regularization matrices for subsequent research. The regularization matrices $\mathbf{L}_1$, $\mathbf{L}_2$ and $\mathbf{L}_3$ are corresponding to CG($\mathbf{L}_1$), M-PCG($\mathbf{L}_2$) and M-PCG($\mathbf{L}_3$), respectively.

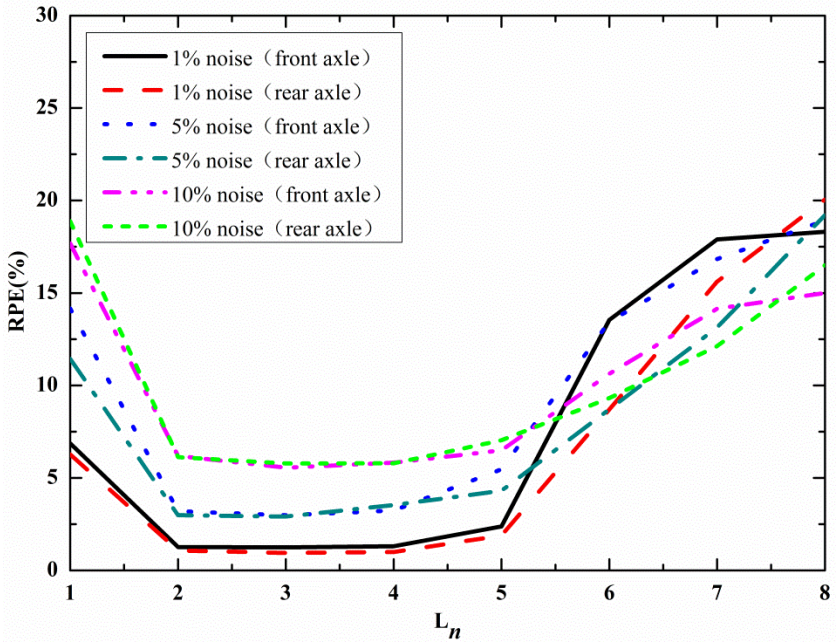

Fig.2. Biaxial time-varying forces identified from combined responses by M-PCG with different regularization matrices (1/2m&1/4a&1/2a)

Table 1
Comparison on RPE values (%) identified by TDM(SVD), CG and M-PCG with two different regularization matrices

Sensor location	regularization matrix **L**	1% noise		5% noise		10% noise	
		front axle	rear axle	front axle	rear axle	front axle	rear axle
1/4m&1/2m	TDM(SVD)	93.5	*	*	*	*	*
	CG($\mathbf{L}_1$)	*26.0*	*21.7*	*33.8*	*28.7*	*42.5*	*39.7*
	M-PCG($\mathbf{L}_2$)	(5.0)	(5.2)	(11.7)	(10.7)	(18.6)	(18.2)
	M-PCG($\mathbf{L}_3$)	4.5	4.2	10.3	9.9	17.3	17.5
1/4m&1/2m&3/4m	TDM(SVD)	50.8	*	*	*	*	*
	CG($\mathbf{L}_1$)	*17.1*	*18.4*	*24.2*	*25.3*	*34.3*	*34.1*
	M-PCG($\mathbf{L}_2$)	(3.3)	(3.1)	(10.4)	(10.8)	(16.9)	(17.2)
	M-PCG($\mathbf{L}_3$)	3.3	3.3	9.8	6.9	16.9	11.3
1/4a&1/2a	TDM(SVD)	19.2	29.7	96.1	*	*	*
	CG($\mathbf{L}_1$)	*7.6*	*2.9*	*12.8*	*13.0*	*16.8*	*16.4*
	M-PCG($\mathbf{L}_2$)	(1.3)	(1.3)	(2.8)	(2.8)	(5.5)	(5.5)
	M-PCG($\mathbf{L}_3$)	1.4	1.7	2.5	2.7	4.3	4.7
1/4a&1/2a&3/4a	TDM(SVD)	0.5	1.0	2.4	5.1	4.7	10.1
	CG($\mathbf{L}_1$)	*0.5*	*1.1*	*2.4*	*5.1*	*4.7*	*10.2*
	M-PCG($\mathbf{L}_2$)	(0.5)	(0.9)	(1.8)	(1.5)	(2.7)	(3.3)
	M-PCG($\mathbf{L}_3$)	0.4	0.9	1.6	2.5	2.8	3.8
1/2m&1/2a	TDM(SVD)	86.3	94.7	*	*	*	*
	CG($\mathbf{L}_1$)	*14.0*	*16.1*	*18.2*	*20.7*	*20.3*	*22.9*
	M-PCG($\mathbf{L}_2$)	(2.6)	(3.7)	(7.9)	(7.5)	(10.2)	(9.2)
	M-PCG($\mathbf{L}_3$)	3.1	3.6	10.2	7.6	12.8	9.4
1/4m&1/2m&1/2a	TDM(SVD)	54.6	48.5	*	*	*	*
	CG($\mathbf{L}_1$)	*14.1*	*15.2*	*18.1*	*20.7*	*22.1*	*22.6*
	M-PCG($\mathbf{L}_2$)	(2.4)	(3.5)	(7.2)	(7.1)	(9.6)	(10.3)
	M-PCG($\mathbf{L}_3$)	2.5	2.6	7.9	10.7	12.2	12.0
1/4m&1/2m&1/4a&1/2a	TDM(SVD)	11.7	15.0	58.6	74.9	*	*
	CG($\mathbf{L}_1$)	*7.8*	*3.0*	*14.2*	*12.1*	*17.8*	*19.3*
	M-PCG($\mathbf{L}_2$)	(1.3)	(1.4)	(2.8)	(3.0)	(5.2)	(4.6)

1/4m&1/4a	M-PCG($\mathbf{L}_3$)	1.2	1.5	2.8	4.4	5.2	5.9
	TDM(SVD)	*	*	*	*	*	*
	CG($\mathbf{L}_1$)	*15.4*	*15.5*	*19.4*	*22.8*	*29.3*	*23.8*
	M-PCG($\mathbf{L}_2$)	(3.7)	(5.5)	(6.0)	(5.5)	(6.7)	(7.2)
	M-PCG($\mathbf{L}_3$)	3.0	4.8	9.9	7.3	9.7	8.1
1/4m&1/4a&1/2a	TDM(SVD)	18.4	29.0	91.9	*	*	*
	CG($\mathbf{L}_1$)	*7.9*	*3.4*	*14.3*	*12.2*	*17.2*	*18.7*
	M-PCG($\mathbf{L}_2$)	(1.4)	(1.4)	(2.3)	(3.0)	(4.1)	(4.2)
	M-PCG($\mathbf{L}_3$)	1.6	1.3	2.3	4.3	4.3	5.5
1/2m&1/4a	TDM(SVD)	48.1	84.0	*	*	*	*
	CG($\mathbf{L}_1$)	*16.8*	*17.2*	*23.5*	*23.6*	*27.5*	*27.2*
	M-PCG($\mathbf{L}_2$)	(4.6)	(4.8)	(6.5)	(6.9)	(6.8)	(8.4)
	M-PCG($\mathbf{L}_3$)	4.6	4.6	10.9	8.9	11.3	10.5
1/4m&1/2m&1/4a	TDM(SVD)	44.3	71.0	*	*	*	*
	CG($\mathbf{L}_1$)	*15.6*	*14.6*	*21.5*	*21.2*	*26.2*	*24.5*
	M-PCG($\mathbf{L}_2$)	(3.8)	(3.6)	(6.4)	(6.5)	(7.1)	(8.0)
	M-PCG($\mathbf{L}_3$)	2.8	4.1	7.4	7.6	11.1	10.3
1/2m&1/4a&1/2a	TDM(SVD)	11.9	15.0	59.5	74.7	*	*
	CG($\mathbf{L}_1$)	*8.1*	*3.5*	*14.2*	*11.7*	*17.7*	*18.9*
	M-PCG($\mathbf{L}_2$)	(1.4)	(1.1)	(3.1)	(2.9)	(6.4)	(6.1)
	M-PCG($\mathbf{L}_3$)	1.4	0.9	2.9	3.2	5.6	5.8

Note: 1/4, 1/2 and 3/4 represent the measurement location at a quarter, middle span and three quarters respectively. The letters 'm' and 'a' represent the bending moment and acceleration responses respectively. Upright font values are for TDM with SVD technique, italics font values are for CG with unit matrix $\mathbf{L}_1$, the values in parentheses are for M-PCG with double diagonal matrix $\mathbf{L}_2$, underlined font values are for M-PCG with tri-diagonal matrix $\mathbf{L}_3$. The symbol '*' represent the RPE is bigger than 100% in which the identification results are unacceptable.

The conventional counterpart SVD has embedded in the time domain method TDM to improve the identification accuracy [17]. Table 1 tabulates the RPE values of TDM with SVD technique, CG and M-PCG with two different regularization matrices in 12 cases. The identification results of TDM(SVD) are the worst and most RPE values are bigger than 100% when noise level is higher than 5% in 12 cases. When CG($\mathbf{L}_1$) is used to identify the moving forces, the RPE values are less than 30% in 10 cases out of all 12 cases with three random noise levels choosing as 1%, 5% and 10%, respectively, which has more acceptable identification accuracy. When M-PCG($\mathbf{L}_2$) and M-PCG($\mathbf{L}_3$) are used to identify the moving forces, the RPE values are less than 20% in all 12 cases with three random noise levels. In addition, with the noise level increasing, the RPE values of the M-PCG increase slightly indicating that the M-PCG($\mathbf{L}_2$) and M-PCG($\mathbf{L}_3$) have good robustness.

As shown in Fig.3 to Fig.5, the identification results of TDM(SVD) and CG methods are obviously worse compared with M-PCG, especially for the case of TDM(SVD). Similar to the data in Table 1, the illustration results also show that even though the CG method has overall much better identification accuracy than TDM(SVD), this technique still needs identification improvement at certain points such as when both front and rear axles are not simultaneously on the bridge. At these boundary points, the identification results of TDM(SVD) and CG are in fact both subject to large deviations. By choosing suitable regularization matrices of M-PCG, the M-PCG($\mathbf{L}_2$) and M-PCG($\mathbf{L}_3$) have almost overcome the ill-posed problem, which have perfect identification accuracy in the whole period of vehicle passing through the bridge.

More importantly, there are only two responses taken into account in Fig.3 to Fig.5, the identification forces of M-PCG($\mathbf{L}_2$) and M-PCG($\mathbf{L}_3$) are in strong agreement with the true forces even under various combined responses, which means that the M-PCG has perfect adaptability to type of sensors and numbers of sensors.

Considering altogether the RPE values of M-PCG($\mathbf{L}_2$) and M-PCG($\mathbf{L}_3$) in all 12 cases, the RPE values of M-PCG($\mathbf{L}_3$) are relatively smaller than M-PCG($\mathbf{L}_2$) when moving forces are identified from bending moment responses alone, which means that the M-PCG($\mathbf{L}_3$) has better adaptability to type of sensors. As a result, the matrix $\mathbf{L}_3$ is selected as the optimal regularization matrix for M-PCG, which is case independent and will be used by default in subsequent studies. It should be noted that in this section the optimal numbers of iterations are adopted to study the effect of regularization matrix whilst the problem of how to select the optimal numbers of iterations for M-PCG will be studied in section 3.4.

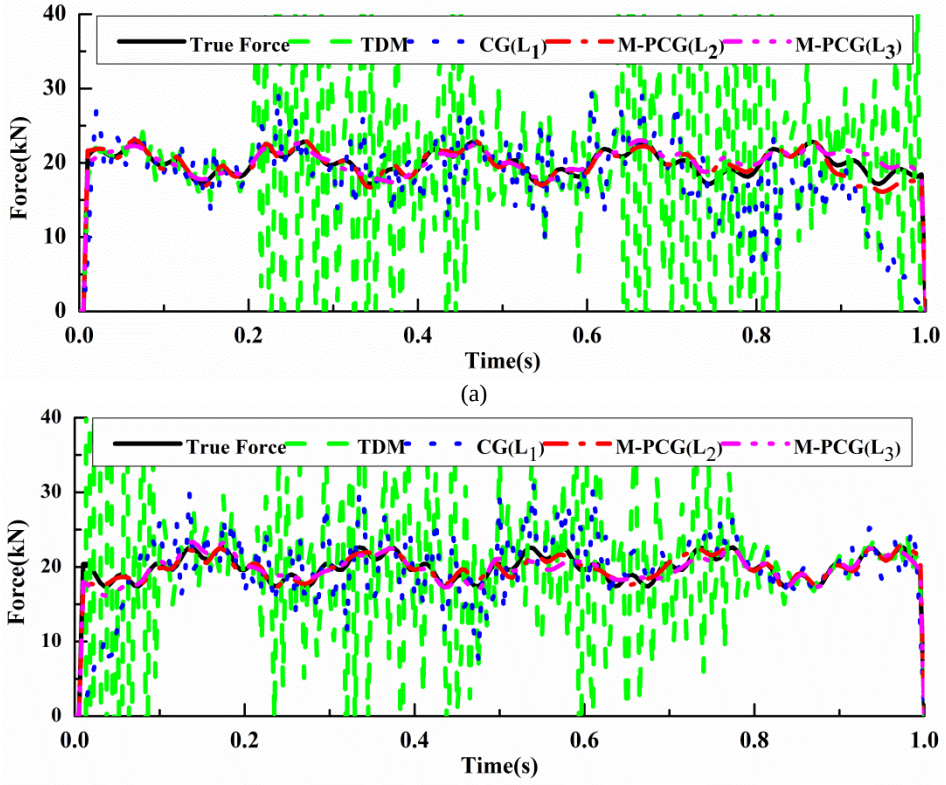

(a)

(b)

Fig.3. MFI from bending moment responses by TDM (SVD), CG and M-PCG with two different regularization matrices (1/4m&1/2m 1% Noise). (a) Front axle; (b) Rear axle.

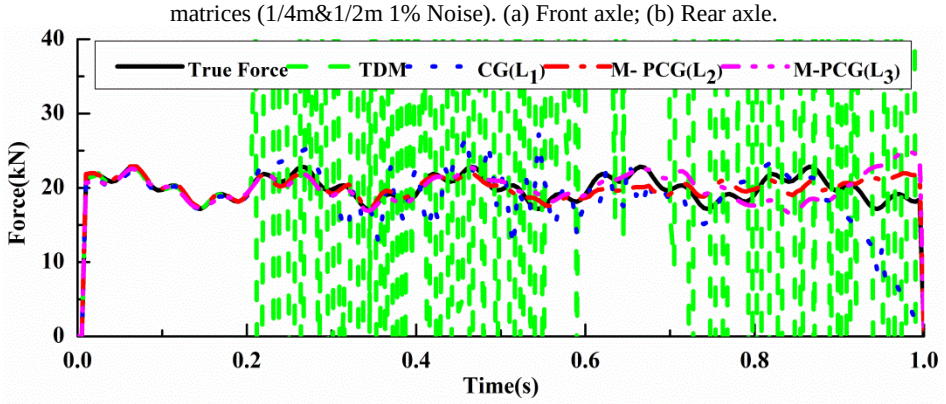

(a)

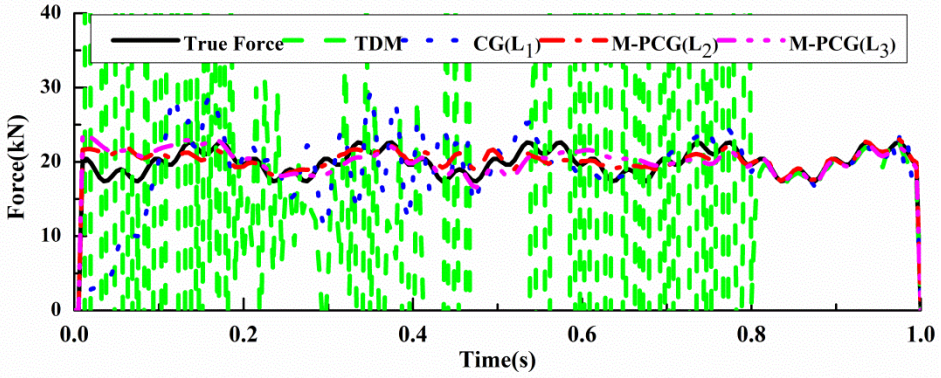

(b)

Fig.4. MFI from combined responses by TDM (SVD), CG and M-PCG with two different regularization matrices (1/4m&1/4a 5% Noise). (a) Front axle; (b) Rear axle.

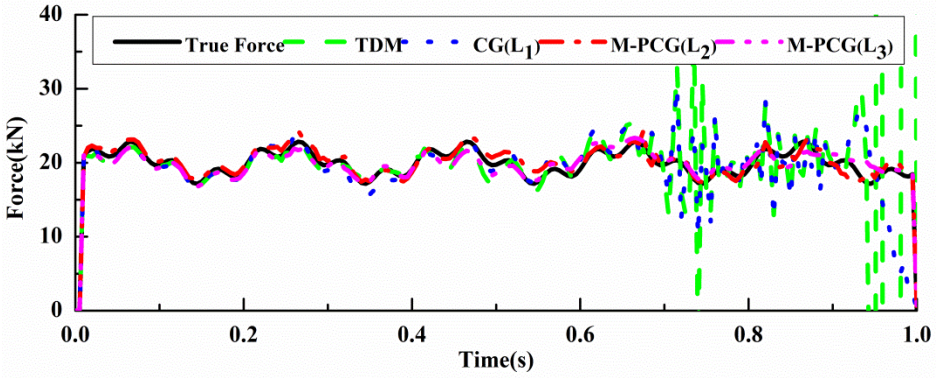

(a)

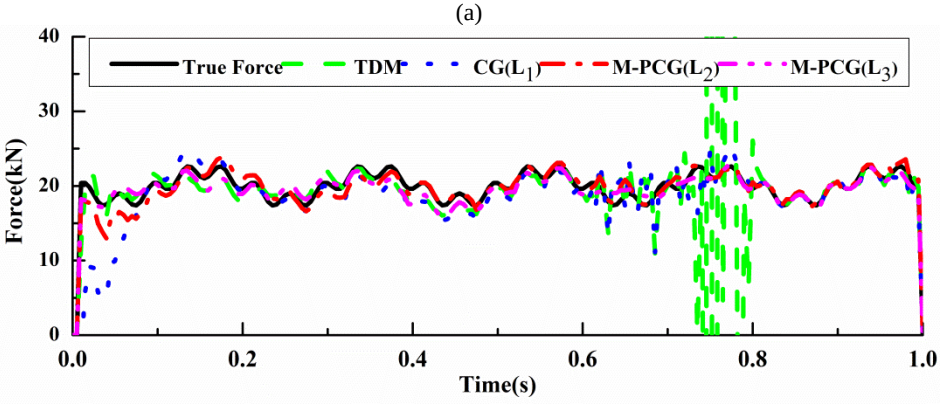

(b)

Fig.5. MFI from acceleration responses by TDM (SVD), CG and M-PCG with two different regularization matrices (1/4a&1/2a 10% Noise). (a) Front axle; (b) Rear axle.

3.3. Evaluation of M-PCG against PCG

Table 2

Comparison on RPE values (%) and optimal numbers of iterations of PCG and M-PCG

Sensor location	1% noise				5% noise				10% noise			
	*j*1	RPE	*j*2	RPE	*j*1	RPE	*j*2	RPE	*j*1	RPE	*j*2	RPE
1/4m&1/2m	228	4.6 (4.1)	*39*	4.5 (4.2)	37	10.3 (9.9)	*18*	10.3 (9.9)	37	17.3 (17.5)	*18*	17.3 (17.5)
1/4m&1/2m&3/4m	352	3.3 (3.8)	*39*	3.3 (3.3)	41	9.7 (6.8)	*19*	9.8 (6.9)	41	16.9 (11.2)	*19*	16.9 (11.3)
1/4a&1/2a	1030	1.4 (1.7)	*88*	1.4 (1.7)	423	2.4 (2.8)	*64*	2.5 (2.7)	400	4.3 (4.8)	*64*	4.3 (4.7)
1/4a&1/2a&3/4a	608	1.4 (1.0)	*175*	0.4 (0.9)	261	1.5 (2.6)	*65*	1.6 (2.5)	163	2.8 (3.8)	*45*	2.8 (3.8)

1/2m&1/2a	381	3.1 (3.5)	*53*	3.1 (3.6)	261	10.3 (9.1)	*34*	10.2 (7.6)	45	12.8 (9.1)	*22*	12.8 (9.4)
1/4m&1/2m&1/2a	1431	2.5 (2.9)	*98*	2.5 (2.6)	240	7.9 (9.4)	*48*	7.9 (10.7)	33	11.9 (11.5)	*19*	12.2 (12.0)
1/4m&1/2m&1/4a&1/2a	631	1.7 (1.6)	*159*	1.2 (1.5)	501	2.7 (4.5)	*67*	2.8 (4.4)	146	5.2 (5.9)	*43*	5.2 (5.9)
1/4m&1/4a	1130	3.0 (4.8)	*92*	3.0 (4.8)	119	9.9 (7.2)	*38*	9.9 (7.3)	90	10.2 (7.6)	*33*	9.7 (8.1)
1/4m&1/4a&1/2a	571	1.6 (1.6)	*130*	1.6 (1.3)	447	2.2 (4.4)	*68*	2.3 (4.3)	149	4.2 (5.8)	*43*	4.3 (5.5)
1/2m&1/4a	710	4.8 (4.9)	*77*	4.6 (4.6)	66	10.8 (9.0)	*31*	10.9 (8.9)	57	11.5 (10.8)	*27*	11.3 (10.5)
1/4m&1/2m&1/4a	1531	2.8 (4.0)	*98*	2.8 (4.1)	271	7.3 (7.7)	*53*	7.4 (7.6)	48	10.9 (9.7)	*26*	11.1 (10.3)
1/2m&1/4a&1/2a	861	1.4 (1.9)	*149*	1.4 (0.9)	451	3.0 (3.4)	*65*	2.9 (3.2)	448	5.5 (5.9)	*64*	5.6 (5.8)

Note: Upright font values are for PCG with the optimal numbers of iterations $j1$, italics font values are for M-PCG with the optimal numbers of iterations $j2$. The RPE values not in parentheses are for front axle and the RPE values in parentheses are for rear axle, the underlined RPE values are for M-PCG.

It is well known that the computation efficiency and identification accuracy are equally important in the field of MFI. Especially for iterative methods, the numbers of iterations are linearly related to the identification time. Reducing the optimal numbers of iterations can effectively reduce the calculation time and the computation cost of MFI. Therefore, it is necessary to examine the computation efficiency of the M-PCG method against the PCG method. As mentioned earlier, one improvement of M-PCG over PCG is the addition of MGS iterative orthogonalization.

Table 2 tabulates the RPE values of PCG and M-PCG with corresponding optimal numbers of iterations in all 12 cases. As shown in Table 2, the computation efficiency of M-PCG is significantly improved compared with PCG. When noise level is 1%, 5% and 10%, the average optimal numbers of iterations of M-PCG in 12 cases reduces by 87.4%, 81.7% and 74.4% compared with PCG, respectively. Fig.6 also demonstrates that the optimal numbers of iterations obviously decrease with the increasing of noise level from 1% to 10%, which has same rule for both methods.

As shown in Fig.7 to Fig.9 and Table 2, the identification accuracy of PCG and M-PCG are very close with each other in all cases. The identified forces of PCG and M-PCG are in strong agreement with the true forces even under various combined responses. Both of the methods have excellent robustness to response noise and ill-posedness problem, the M-PCG is recommended for field MFI applications due to its superior efficiency in computation.

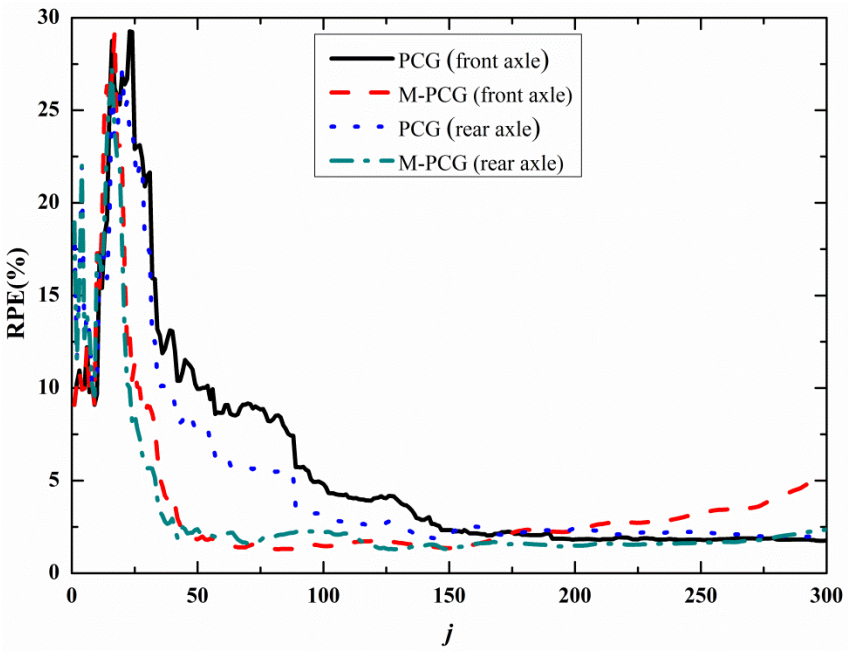
PCG (front axle)
M-PCG (front axle)
PCG (rear axle)
M-PCG (rear axle)
RPE(%)
j
0
5
10
15
20
25
30
0
50
100
150
200
250
300

(a)

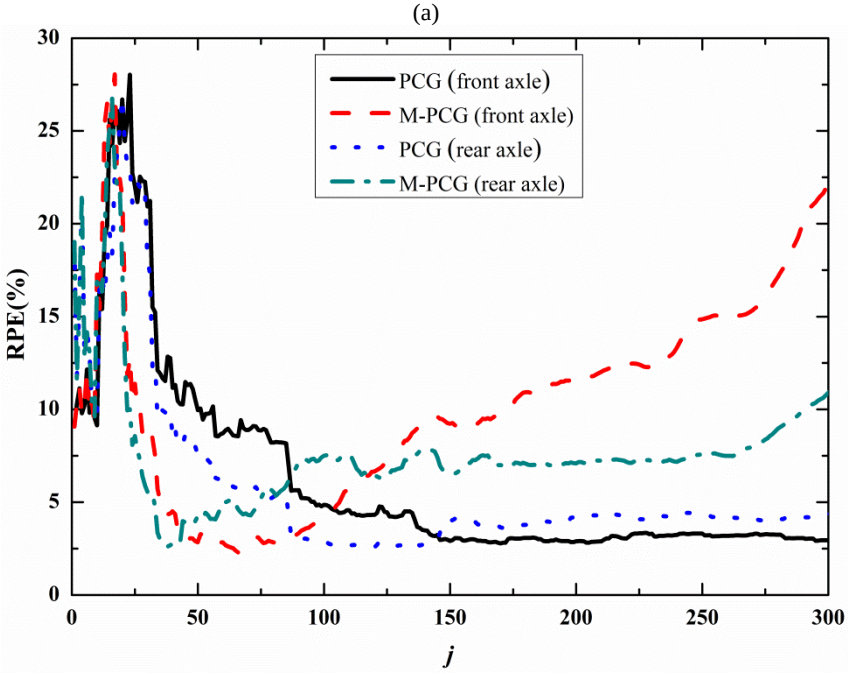
PCG (front axle)
M-PCG (front axle)
PCG (rear axle)
M-PCG (rear axle)
RPE(%)
j
0
5
10
15
20
25
30
0
50
100
150
200
250
300

(b)

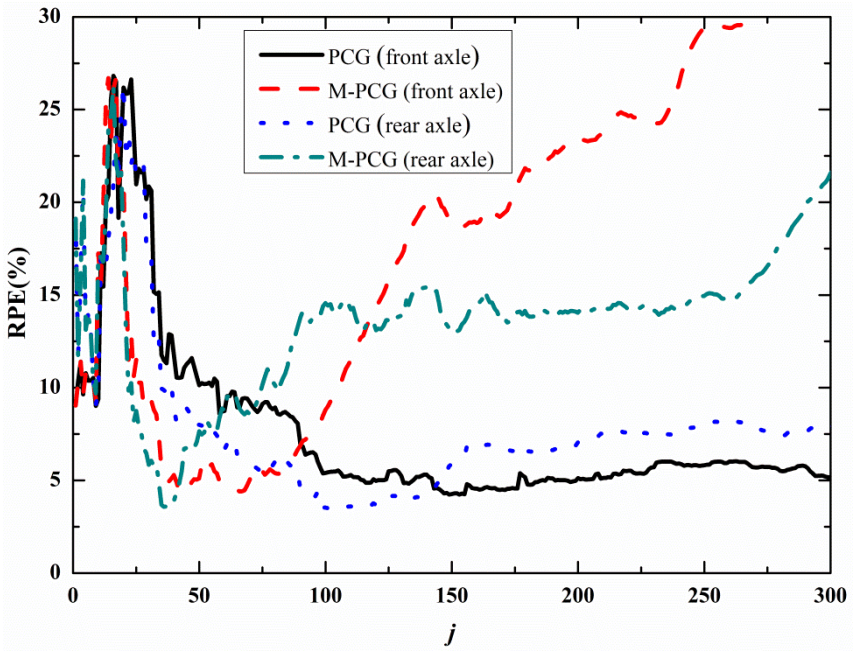

(c)

Fig.6. Influence of numbers of iterations *j* of PCG and M-PCG with three noise levels (1/4m&1/4a&1/2a). (a) 1% Noise; (b) 5% Noise; (c) 10% Noise.

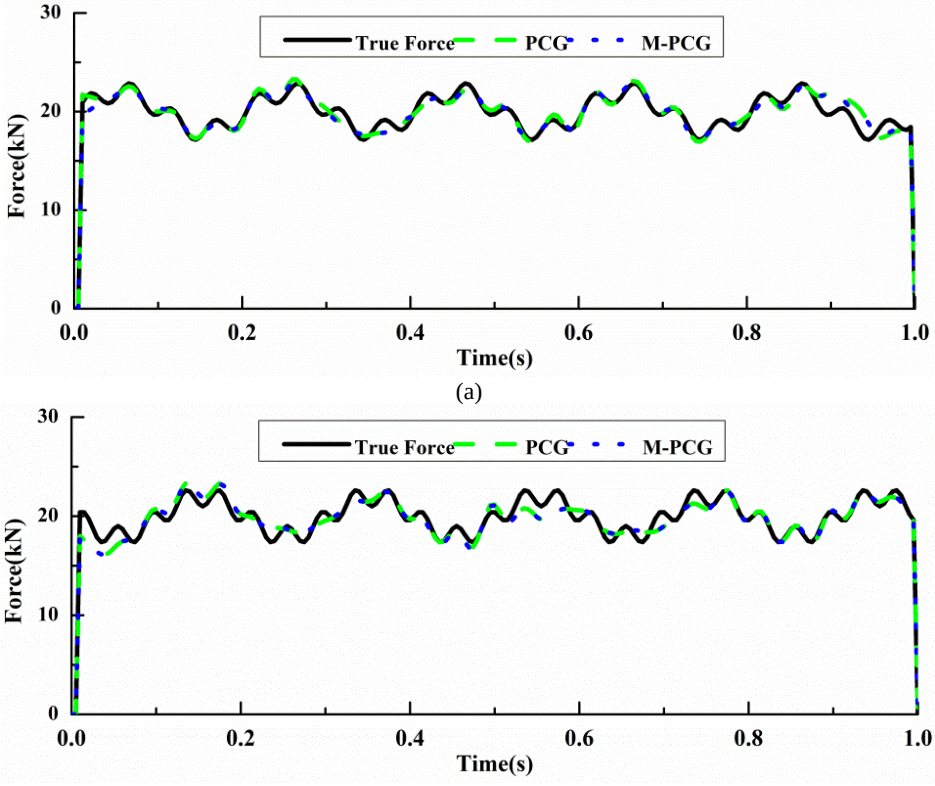

(a)

(b)

Fig.7. Identified biaxial time-varying forces with PCG and M-PCG from bending moment responses (1/4m&1/2m&3/4m 1% Noise). (a) Front axle; (b) Rear axle.

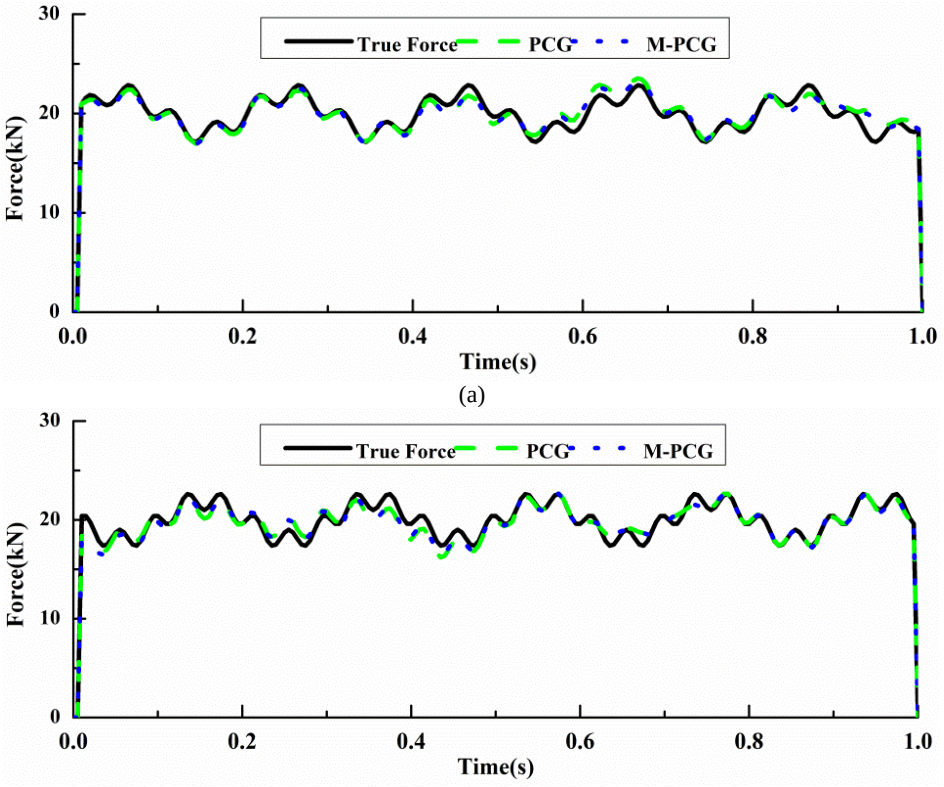

(a)

(b)

Fig.8. Identified biaxial time-varying forces with PCG and M-PCG from combined responses (1/2m&1/4a&1/2a 5% Noise). (a) Front axle; (b) Rear axle.

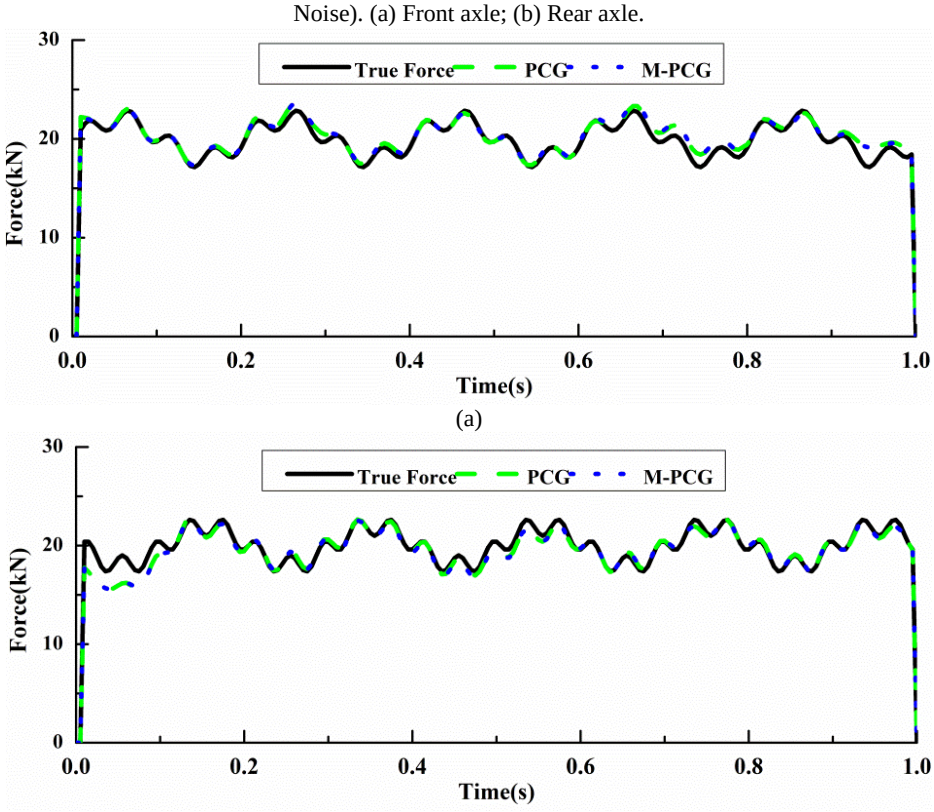

(a)

(b)

Fig.9. Identified biaxial time-varying forces with PCG and M-PCG from acceleration responses (1/4a&1/2a&3/4a 10% Noise). (a) Front axle; (b) Rear axle.

3.4. Choosing optimal numbers of iterations j for M-PCG

Table 3

Comparison on RPE values (%) of M-PCG($\mathbf{L}_3$) with three different numbers of iterations

Sensor location	axle	1% noise			5% noise			10% noise		
		$j1$	$j2$	$j3$	$j1$	$j2$	$j3$	$j1$	$j2$	$j3$
1/4m&1/2m	front	11.7	4.5	(5.6)	15.6	10.3	(16.0)	24.8	17.3	(22.3)
	rear	9.2	4.2	(3.9)	12.4	9.9	(14.3)	19.0	17.5	(21.0)
1/4m&1/2m&3/4m	front	10.2	3.3	(3.4)	15.1	9.8	(14.7)	21.7	16.9	(21.4)
	rear	10.8	3.3	(3.4)	14.9	6.9	(10.3)	20.7	11.3	(20.5)
1/4a&1/2a	front	28.7	1.4	(4.2)	28.2	2.5	(5.3)	27.6	4.3	(6.7)
	rear	27.5	1.7	(3.3)	28.0	2.7	(4.4)	28.4	4.7	(6.0)
1/4a&1/2a&3/4a	front	20.1	0.4	(2.5)	20.7	1.6	(3.1)	20.9	2.8	(3.8)
	rear	24.4	0.9	(1.5)	23.9	2.5	(2.1)	23.4	3.8	(3.0)
1/2m&1/2a	front	35.5	3.1	(6.0)	36.2	10.2	(10.7)	37.3	12.8	(19.6)
	rear	31.2	3.6	(4.2)	31.8	7.6	(7.7)	32.6	9.4	(15.4)
1/4m&1/2m&1/2a	front	30.3	2.5	(4.7)	30.4	7.9	(8.5)	30.8	12.2	(15.0)
	rear	28.9	2.6	(2.6)	29.6	10.7	(6.9)	31.2	12.0	(14.8)
1/4m&1/2m&1/4a&1/2a	front	24.8	1.2	(4.3)	25.0	2.8	(4.9)	25.2	5.2	(6.2)
	rear	24.9	1.5	(2.5)	25.9	4.4	(2.9)	25.9	5.9	(4.7)
1/4m&1/4a	front	23.3	3.0	(6.1)	25.1	9.9	(10.3)	25.4	9.7	(17.3)
	rear	25.3	4.8	(7.7)	26.1	7.3	(6.9)	26.8	8.1	(12.0)
1/4m&1/4a&1/2a	front	23.3	1.6	(4.3)	24.3	2.3	(4.5)	25.2	4.3	(5.3)
	rear	24.7	1.3	(3.0)	25.2	4.3	(3.3)	25.7	5.5	(4.9)
1/2m&1/4a	front	52.5	4.6	(7.6)	53.6	10.9	(12.7)	53.4	11.3	(19.3)
	rear	43.7	4.6	(6.3)	45.4	8.9	(10.6)	45.7	10.5	(16.6)
1/4m&1/2m&1/4a	front	22.2	2.8	(8.6)	23.3	7.4	(12.8)	23.5	11.1	(18.5)
	rear	26.1	4.1	(7.7)	27.5	7.6	(9.1)	28.2	10.3	(14.7)
1/2m&1/4a&1/2a	front	21.3	1.4	(4.2)	21.9	2.9	(5.6)	21.6	5.6	(7.8)
	rear	23.0	0.9	(3.1)	23.6	3.2	(4.2)	24.0	5.8	(6.3)

Note: Upright font values are for M-PCG($\mathbf{L}_3$) with the worst number of iterations $j1 = 15$, underlined font values are for M-PCG($\mathbf{L}_3$) with the optimal numbers of iterations $j2$ as shown in Table 2, the values in parentheses are for M-PCG($\mathbf{L}_3$) with number of iterations $j3 = 40$.

Table 3 tabulates the RPE values of M-PCG($\mathbf{L}_3$) with three different numbers of iterations in all 12 cases. As shown in Fig.10, when moving forces are identified from bending moment responses alone with high noise level, the larger number of iterations, the greater increase in RPE. The RPE values exceed 40% when the number of iterations exceeds 60 with 10% noise level. Therefore, choosing the optimal numbers of iterations is helpful to improve the identification accuracy of the M-PCG.

In addition to selecting the optimal numbers of iterations $j2$ (the $j2$ values of 12 cases can be found in the former Table 2 with italics font), there are two other numbers of iterations $j1 = 15$ and $j3 = 40$ are chosen for comparing research as the following reasons.

As shown in Fig.10 to Fig.13, when the number of iterations is 15, the RPE curves have a distinct peak, and then the worst number of iterations $j1 = 15$ is adopted to explore the causes of the excessively high RPE values as the ill-posed problems. It also can be shown in Fig.12 and Fig.13, if more than two acceleration responses are contained for MFI, the RPE values maintain over a long range of numbers of iterations from 40 to 300. With the increase of the numbers of iterations, the identification accuracy is not improved obviously. Therefore, it is not worth to find the optimal numbers of iterations while increase the calculation time and the identification cost, and then the stable number of iterations $j3 = 40$ is adopted to

explore whether it can be adopted as reasonable number of iterations of M-PCG to avoid choosing the optimal numbers of iterations.

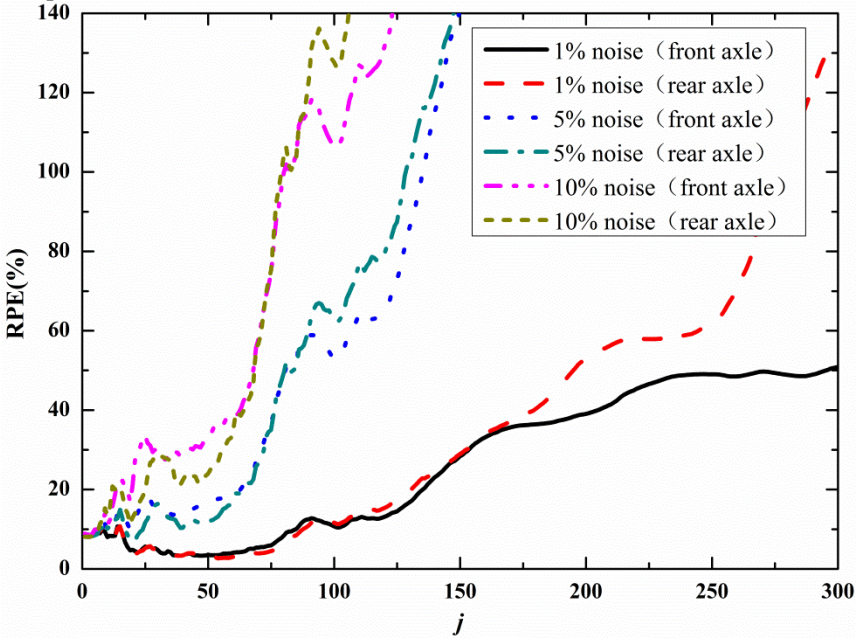

Fig.10. Influence of numbers of iterations j of M-PCG($\mathbf{L}_3$) on MFI from bending moment responses (1/4m&1/2m&3/4m)

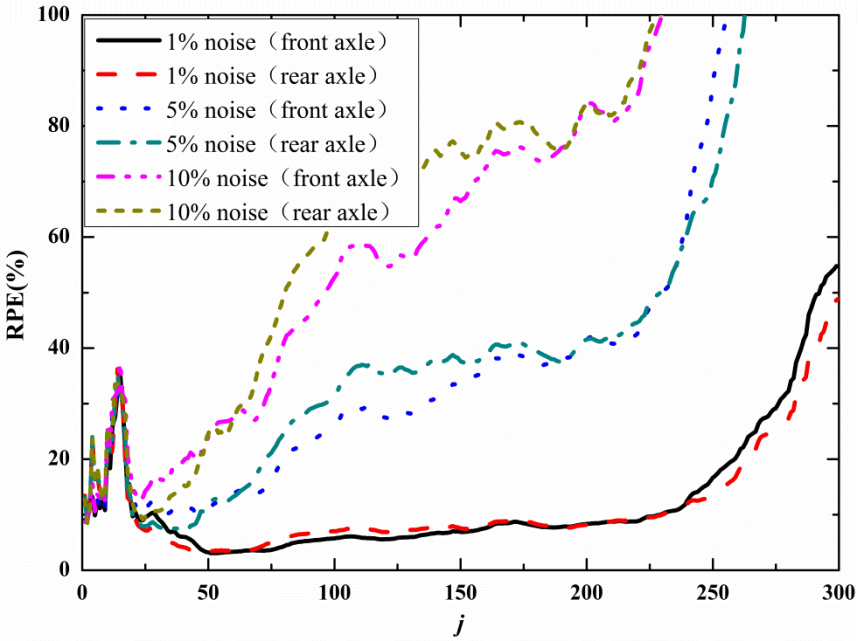

Fig.11. Influence of numbers of iterations j of M-PCG($\mathbf{L}_3$) on MFI from combined responses (1/2m&1/2a)

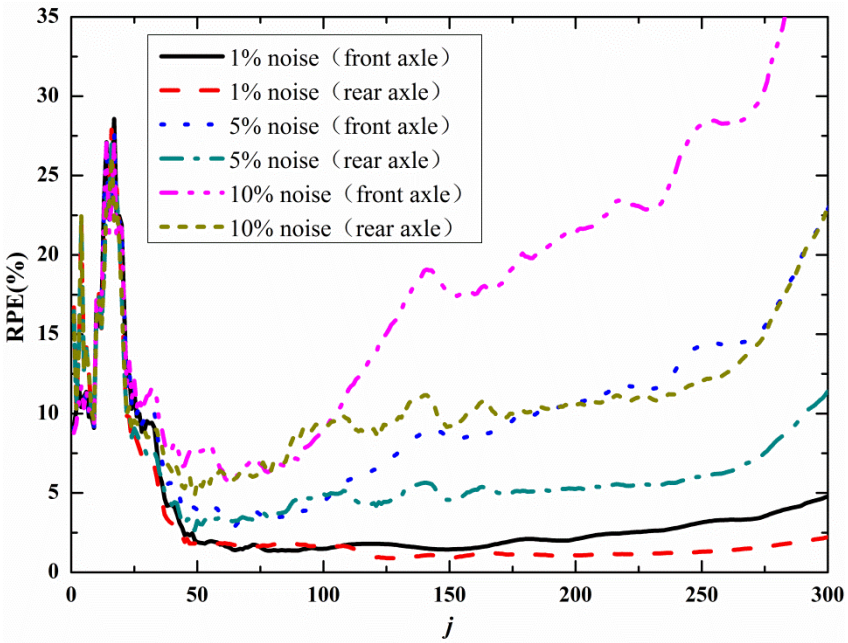

Fig.12. Influence of numbers of iterations j of M-PCG($\mathbf{L}_3$) on MFI from combined responses (1/2m&1/4a&1/2a)

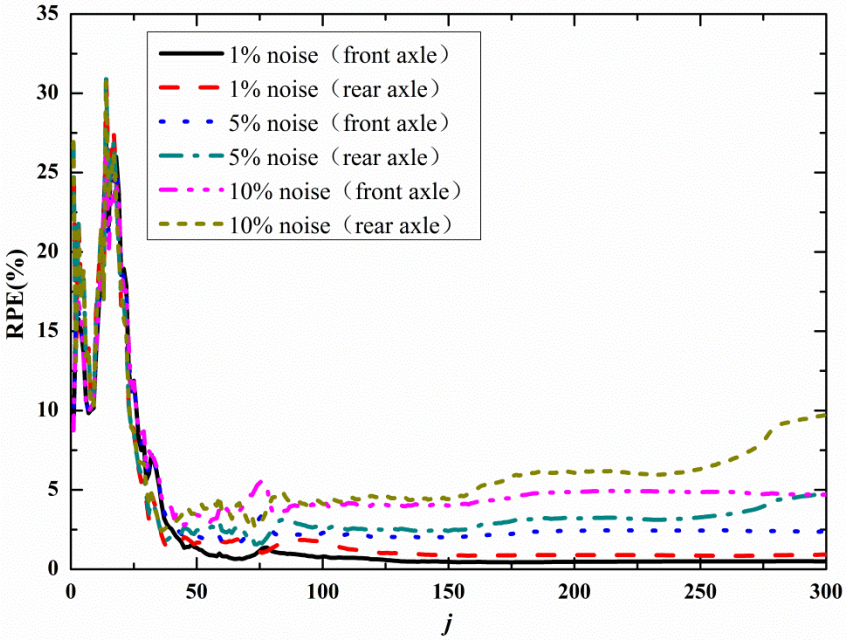

Fig.13. Influence of numbers of iterations j of M-PCG($\mathbf{L}_3$) on MFI from acceleration responses (1/4a&1/2a&3/4a)

As shown in Fig.14 to Fig.16, the RPE values of M-PCG($\mathbf{L}_3$) are largest with number of iterations $j1 = 15$ compared with $j2$ and $j3 = 40$, especially when both front and rear axles are not simultaneously on the bridge as the ill-posed problems. The RPE values have little change with different noise level and the identified forces have great deviation to true forces, and then the use of number of iterations at 15 should be avoided for M-PCG($\mathbf{L}_3$).

When the optimal numbers of iterations $j2$ is adopted, the identification results are most accurate, which is the closest to the true forces. When the stable number of iterations $j3 = 40$ is adopted, the identification results also very close to the true forces as shown in Table 3 and Fig.14 to Fig.16. It means that when the optimal numbers of iterations cannot be reasonably determined without knowing the actual moving forces, the number of iterations $j3 = 40$ can

be adopted as a reasonable number of iterations of M-PCG($\mathbf{L}_3$) to facilitate MFI. Some other simulations with different MFI examples have shown that the stable number of iterations is directly related with the number of columns of vehicle-bridge system matrix **A**, which can be selected as 10% of the number of columns of matrix **A**.

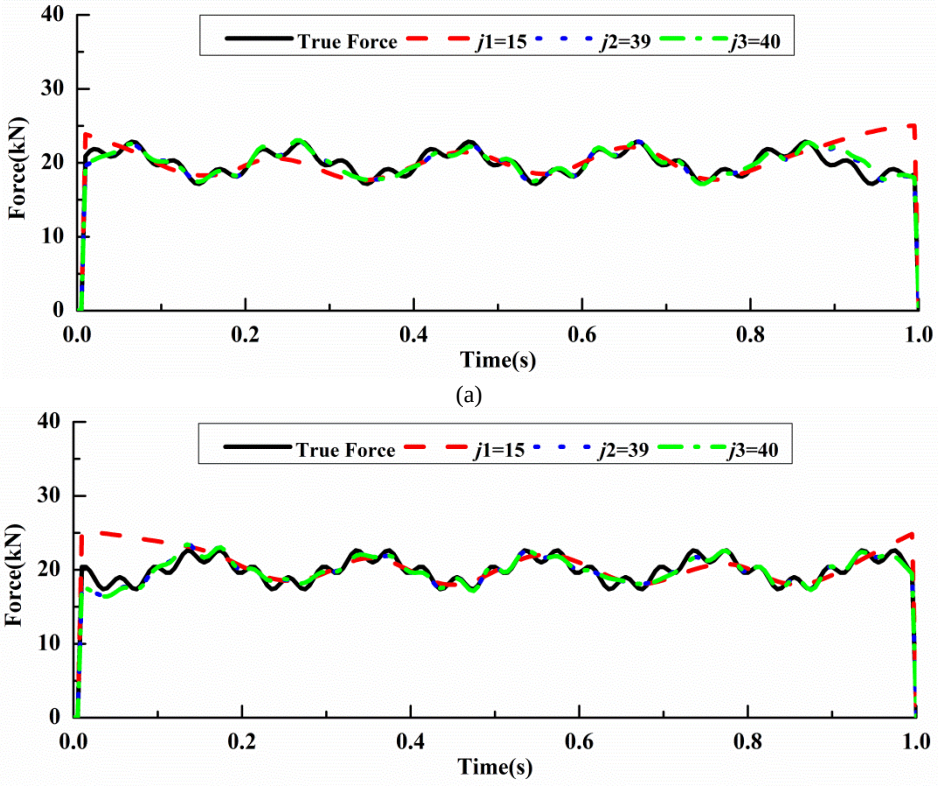

(a)

(b)

Fig.14. MFI from bending moment responses by M-PCG($\mathbf{L}_3$) with three different numbers of iterations *j* (1/4m&1/2m&3/4m 1% Noise). (a) Front axle; (b) Rear axle.

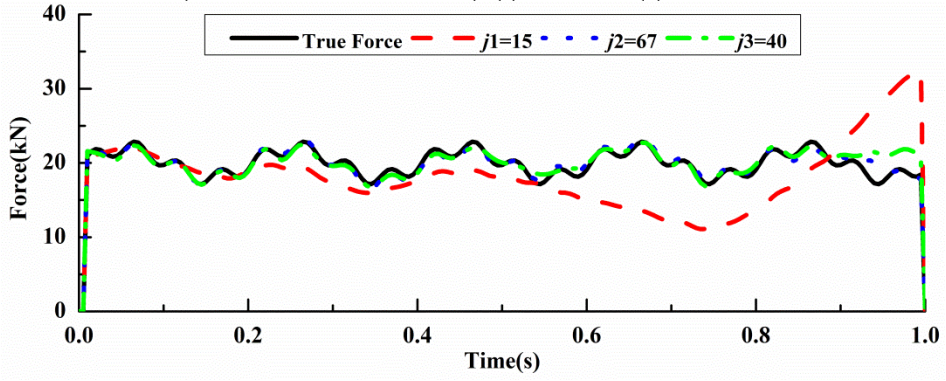

(a)

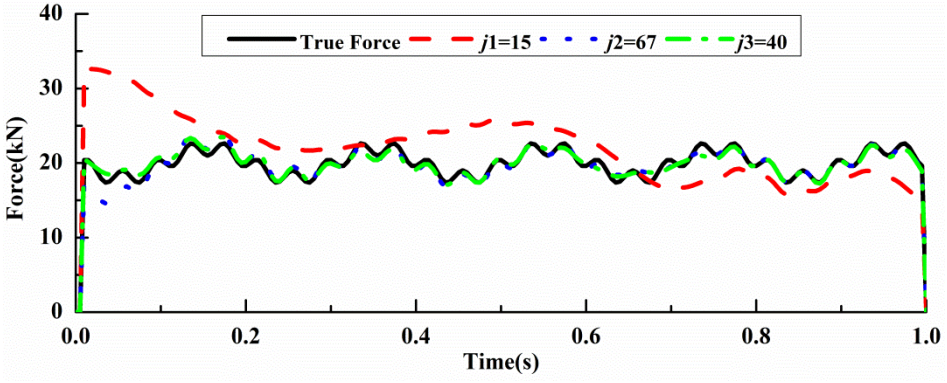

(b)

Fig.15. MFI from combined responses by M-PCG($\mathbf{L}_3$) with three different numbers of iterations j (1/4m&1/2m&1/4a&1/2a 5% Noise). (a) Front axle; (b) Rear axle.

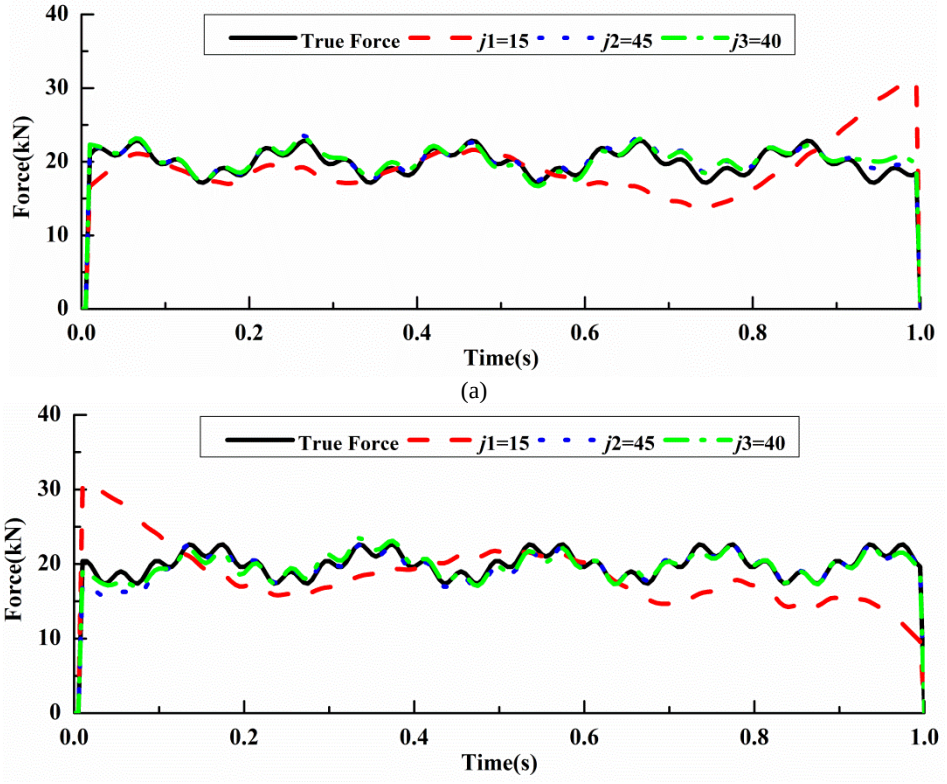

(a)

(b)

Fig.16. MFI from acceleration responses by M-PCG($\mathbf{L}_3$) with three different numbers of iterations j (1/4a&1/2a&3/4a 10% Noise). (a) Front axle; (b) Rear axle.

4. Conclusions

In this work, a method named M-PCG is proposed for MFI based on CG and PCG methods incorporated MGS algorithm. Moreover, this paper proposes qualitative and quantitative selection rules about parameters that affect the accuracy of the M-PCG, such as regularization matrix $\mathbf{L}$ and number of iterations j. When M-PCG($\mathbf{L}_2$) and M-PCG($\mathbf{L}_3$) are used to identify the moving forces, the identification accuracy is significantly improved compared with TDM(SVD) and CG ($\mathbf{L}_1$) in all 12 cases. The M-PCG can overcome most ill-posed problems of CG, through choosing proper regularization matrix. It is shown that when the optimal numbers of iterations cannot be determined prior, the number of iterations $j3 = 40$ can be

adopted as a reasonable number of iterations to facilitate the MFI procedure. On the contrary, the number of iterations $j1 = 15$ should be avoided as it amplifies the ill-posed problems. In comparison with similar methods such as PCG, the computation efficiency of M-PCG is shown to be superior while retaining the same identification accuracy and robustness against response noise and the ill-posedness problem. These advantages obviously make the M-PCG a preferred candidate for computationally intensive MFI applications such as those for medium to large-scale bridges.

Acknowledgments

This research was financially supported by key research project of higher education of Henan Province, China (Grant no.17A560006) and science and technology innovation team of eco-building material and structural engineering in the university of Henan Province, China (Grant no.13IRTSTHN002).

References:

[1] P. Chatterjee, E.J. OBrien, Y.Y. Li, A. González, Wavelet domain analysis for identification of vehicle axles from bridge measurements, Comput. Struct. 84 (2006) 1792-1801.
[2] S. Abhinav, C.S. Manohar, Substructuring tools for probabilistic analysis of instrumented nonlinear moving oscillator-beam systems, Appl. Math. Model. 42 (2017) 600-617.
[3] J. Liu, X.S. Sun, X. Han, C. Jiang, D.J. Yu, A novel computational inverse technique for load identification using the shape function method of moving least square fitting, Comput. Struct. 144 (2014) 127-137.
[4] C. O'Connor, T.H.T. Chan, Dynamic wheel loads from bridge strains, J. Struct. Eng. 114(8) (1988) 1703-1723.
[5] T.H.T. Chan, S.S. Law, T.H. Yung, X.R. Yuan, An interpretive method for moving force identification, J. Sound Vib. 219(3) (1999) 503-524.
[6] S.S. Law, T.H.T. Chan, Q.H. Zeng, Moving force identification: a time domain method, J. Sound Vib. 201(1) (1997) l-22.
[7] S.S. Law, T.H.T. Chan, Q.H. Zeng, Moving force identification-a frequency and time domains analysis, ASME J. Dyn. Syst. Meas. Control 121(3) (1999) 394-401.
[8] T.H.T. Chan, L. Yu, S.S. Law, T.H. Yung, Moving force identification studies I: theory, J. Sound Vib. 247(1) (2001) 59-76.
[9] T.H.T. Chan, L. Yu, S.S. Law, T.H. Yung, Moving force identification studies II: comparative studies, J. Sound Vib. 247(1) (2001) 77-95.
[10] T.H.T. Chan, D.B. Ashebo, Moving axle load from multi-span continuous bridge: Laboratory study, J. Vib. Acoust. 128(4) (2006) 521-526.
[11] X.Q. Zhu, S.S. Law, Moving load identification on multi-span continuous bridges with elastic bearings, Mech. Syst. Signal Process. 20 (2006) 1759-1782.
[12] L. Yu, T.H.T. Chan, Recent research on identification of moving loads on bridges, J. Sound Vib. 305 (2007) 3-21.
[13] S.S. Law, T.H.T. Chan, X.Q. Zhu, Q.H. Zeng, Regularization in moving force identification, J. Eng. Mech. 127(2) (2001) 136-148.
[14] X.Q. Zhu, S.S. Law, Identification of vehicle axle loads from bridge dynamic responses, J. Sound Vib. 236(4) (2000) 705-724.
[15] X.Q. Zhu, S.S. Law, Identification of moving interaction forces with incomplete velocity information, Mech. Syst. Signal Process. 17(6) (2003) 1349-1366.
[16] L. Yu, T.H.T. Chan, Moving force identification based on the frequency-time domain method, J. Sound Vib. 261 (2003) 329-349.
[17] T.H.T. Chan, D.B. Ashebo, Theoretical study of moving force identification on continuous bridges, J. Sound Vib. 295 (2006) 870-883.
[18] X.Q. Jiang, H.Y. Hu, Reconstruction of distributed dynamic loads on an Euler beam via mode-selection and consistent spatial expression, J. Sound Vib. 316 (2008) 122-136.
[19] J. Sanchez, H. Benaroya, Review of force reconstruction techniques, J. Sound Vib. 333 (2014) 2999-3018.
[20] T. Pinkaew, Identification of vehicle axle loads from bridge responses using updated static component technique, Eng. Struct. 28 (2006) 1599-1608.
[21] A. González, C. Rowley, E.J. Obrien, A general solution to the identification of moving vehicle forces on a bridge, Int. J. Numer. Methods Eng. 75(3) (2008) 335-354.

[22] L. Yu, T.H.T. Chan, J.H. Zhu, A MOM-based algorithm for moving force identification: part I-theory and numerical simulation, Struct. Eng. Mech. 29(2) (2008) 135-154.
[23] C.D. Pan, L. Yu, H.L. Liu, Z.P. Chen, W.F. Luo, Moving force identification based on redundant concatenated dictionary and weighted l1-norm regularization, Mech. Syst. Signal Process. 98 (2018) 32-49.
[24] S.Q. Wu, S.S. Law, Moving force identification based on stochastic finite element model, Eng. Struct. 32 (2010) 1016-1027.
[25] J. Dowling, E.J. Obrien, A. González, Adaptation of cross entropy optimization to a dynamic bridge WIM calibration problem, Eng. Struct. 44 (2012) 13-22.
[26] D.M. Feng, H. Sun, M.Q. Feng, Simultaneous identification of bridge structural parameters and vehicle loads, Comput. Struct. 157 (2015) 76-88.
[27] Z. Chen, T.H.T. Chan, A truncated generalized singular value decomposition algorithm for moving force identification with ill-posed problems, J. Sound Vib. 401(2017) 297-310.
[28] M.R. Hestenes, E. Stiefel, Methods of conjugate gradients for solving linear systems, Journal of Research of the National Bureau of Standards 49(6) (1952) 409-436.
[29] R. Plato, The conjugate gradient method for linear ill-posed problems with operator perturbations, Numer. Algorithms 20 (1999) 1-22.
[30] P. Concus, G.H. Golub, G. Meurant, Block preconditioning for the conjugate gradient method, SIAM J. Sci. Statist. Comput. 6(1) (1985) 220-252.
[31] G. Meurant, Z. Strakoš, The Lanczos and conjugate gradient algorithms in finite precision arithmetic, ACTA Numer. 15 (2006) 471-542.
[32] Z. Chen, L. Yu, Moving load identification based on preconditioned conjugate gradient method, Journal of Yangtze River Scientific Research Institute 25(2) (2008) 69-71.
[33] L. Yu, Z. Chen, Experimental study on ill-conditioning problem in identification of moving vehicle loads on bridges, J. Vib. Shock 26(12) (2007) 6-9.
[34] Z. Chen, L. Yu, Effect of preconditioned matrix on PCGM used for identification of dynamic axle loads on bridge, Journal of Zhejiang University (Engineering Science) 43(7) (2009) 1293-1296.
[35] A. Ruhe, Numerical aspects of gram-schmidt orthogonalization of vectors, Linear Algebra Appl. 52-53 (1983) 591-601.
[36] M. Benzi, C.D. Meyer, M. Tuma, A sparse approximate inverse preconditioner for the conjugate gradient method, SIAM J. Sci. Comput. 17(5) (1996) 1135-1149.
[37] M. Hanke, Regularization with differential operators: An iterative approach, J. Numer. Funct. Anal. Optim. 13 (1992) 523-540.
[38] E. Schmidt, Uber die Auflosung linearer Gleichungen mit unendlich vielen Unbekannten, Rend. Circ. Mat. Palermo. 25 (1) (1908) 53-77.
[39] A. Dax, A modified Gram-Schmidt algorithm with iterative orthogonalization and column pivoting, Linear Algebra Appl. 310 (2000) 25-42.
[40] R. Pytlak, Conjugate gradient algorithms in nonconvex optimization, Springer Berlin Heidelberg, 2009.
[41] J.R. Rice, Experiments on Gram-Schmidt orthogonalization, Math. Comp. 20 (1966) 325-328.